## Title

Recoil-α-fission and recoil-α–α-fission events observed in the reaction 48Ca + 243Am



## Authors

Forsberg, U
Rudolph, D
Andersson, L-L
et al.

## Publication Date

2016-09-01

## DOI

10.1016/j.nuclphysa.2016.04.025

Peer reviewed

Available online at www.sciencedirect.com

ScienceDirect

Nuclear Physics A 953 (2016) 117–138

NUCLEAR PHYSICS A

www.elsevier.com/locate/nuclphysa

# Recoil-$\alpha$-fission and recoil-$\alpha$–$\alpha$-fission events observed in the reaction $^{48}$Ca + $^{243}$Am

U. Forsberg [a,*], D. Rudolph [a], L.-L. Andersson [b], A. Di Nitto [c], Ch.E. Düllmann [b,c,d], C. Fahlander [a], J.M. Gates [e], P. Golubev [a], K.E. Gregorich [e], C.J. Gross [f], R.-D. Herzberg [g], F.P. Heßberger [b,d], J. Khuyagbaatar [b], J.V. Kratz [c], K. Rykaczewski [f], L.G. Sarmiento [a], M. Schädel [d,h], A. Yakushev [d], S. Åberg [a] D. Ackermann [d], M. Block [b,c,d], H. Brand [d], B.G. Carlsson [a], D. Cox [g], X. Derkx [b,c], J. Dobaczewski [i,j], K. Eberhardt [b,c], J. Even [b,1], J. Gerl [d], E. Jäger [d], B. Kindler [d], J. Krier [d], I. Kojouharov [d], N. Kurz [d], B. Lommel [d], A. Mistry [g,2], C. Mokry [b,c], W. Nazarewicz [f,i,k], H. Nitsche [e], J.P. Omtvedt [l], P. Papadakis [g,3], I. Ragnarsson [a], J. Runke [d], H. Schaffner [d], B. Schausten [d], Yue Shi [f,k], P. Thörle-Pospiech [b,c], T. Torres [d], T. Traut [c], N. Trautmann [c], A. Türler [m], A. Ward [g], D.E. Ward [a], N. Wiehl [b,c]

[a] *Lund University, 22100 Lund, Sweden*
[b] *Helmholtz Institute Mainz, 55099 Mainz, Germany*
[c] *Johannes Gutenberg-Universität Mainz, 55099 Mainz, Germany*
[d] *GSI Helmholtzzentrum für Schwerionenforschung GmbH, 64291 Darmstadt, Germany*
[e] *Lawrence Berkeley National Laboratory, Berkeley, CA 94720, USA*
[f] *Oak Ridge National Laboratory, Oak Ridge, TN 37831, USA*
[g] *University of Liverpool, Liverpool L69 7ZE, United Kingdom*
[h] *Advanced Science Research Center, Japan Atomic Energy Agency, Tokai, Ibaraki 319-1195, Japan*
[i] *University of Warsaw, 00681 Warsaw, Poland*
[j] *Department of Physics, University of York, Heslington, York YO10 5DD, United Kingdom*
[k] *Department of Physics and Astronomy and NSCL/FRIB Laboratory, Michigan State University, East Lansing, MI 48824, USA*

[*] Corresponding author.
*E-mail address:* ulrika.forsberg@nuclear.lu.se (U. Forsberg).
[1] Current address: KVI-Center for Advanced Radiation Technology, University of Groningen, 9747 AA Groningen, The Netherlands.
[2] Current address: Helmholtz Institute Mainz, 55099 Mainz, Germany.
[3] Current address: Department of Physics, University of Jyväskylä, FIN-40014 Jyväskylä, Finland.

http://dx.doi.org/10.1016/j.nuclphysa.2016.04.025

[l] University of Oslo, 0315 Oslo, Norway
[m] Paul Scherrer Institute and University of Bern, 5232 Villigen, Switzerland

Received 10 February 2016; received in revised form 24 March 2016; accepted 13 April 2016

Available online 26 April 2016

**Abstract**

Products of the fusion-evaporation reaction $^{48}$Ca + $^{243}$Am were studied with the TASISpec set-up at the gas-filled separator TASCA at the GSI Helmholtzzentrum für Schwerionenforschung, Darmstadt, Germany. Amongst the detected thirty correlated $\alpha$-decay chains associated with the production of element $Z = 115$, two recoil-$\alpha$-fission and five recoil-$\alpha$–$\alpha$-fission events were observed. The latter five chains are similar to four such events reported from experiments performed at the Dubna gas-filled separator, and three such events reported from an experiment at the Berkeley gas-filled separator. The four chains observed at the Dubna gas-filled separator were assigned to start from the 2$n$-evaporation channel $^{289}$115 due to the fact that these recoil-$\alpha$–$\alpha$-fission events were observed only at low excitation energies. Contrary to this interpretation, we suggest that some of these recoil-$\alpha$–$\alpha$-fission decay chains, as well as some of the recoil-$\alpha$–$\alpha$-fission and recoil-$\alpha$-fission decay chains reported from Berkeley and in this article, start from the 3$n$-evaporation channel $^{288}$115.


*Keywords:* Superheavy elements; Element 115; Uup; $\alpha$ decay; Spontaneous fission

## 1. Introduction

In the quest for enhanced nuclear stability in the region of SuperHeavy Elements (SHE) – frequently defined as those with $Z \geq 104$ – the two elements flerovium (Fl, $Z = 114$) and livermorium (Lv, $Z = 116$) have recently been officially approved and named [1], and just before New Year's Eve 2015 IUPAC announced their approval of the elements with $Z = 113, 115, 117$ and 118 [2,3].

The interpretation of data on odd-$Z$ elements is especially challenging, but, at the same time, the study of nuclei with odd numbers of neutrons and/or protons can also be especially rewarding: The extra hindrance and thus delay for Spontaneous Fission (SF) renders other decay modes such as $\alpha$ decay and Electron Capture (EC) more likely. Consequently, odd-$Z$ nuclei potentially give rise to decay chains with more $\alpha$-decay members than even-$Z$ ones. Additionally, $\alpha$ decay of odd-$A$ or odd–odd nuclei most often proceeds into excited states in the daughter nucleus, because unpaired nucleons typically remain in the same single-particle orbitals as in the $\alpha$-decay parent [4,5]. Observation of electromagnetic decays from these excited states can thus elucidate the low-lying nuclear structure of the daughter [6]. Such experimental studies have recently reached decay chains of element $Z = 115$ [7,8]. Observations of odd-$Z$ elements have been reported up to the newly approved $Z = 117$ – see, for instance, Refs. [9–15] and references therein.

The low-lying nuclear structure of odd-$Z$ nuclei is usually complex, with several states of various spins and different parities, some of which might be isomeric. This easily translates into complex $\alpha$-decay sequences, where different lifetimes and decay energies can be observed in transitions between a particular pair of mother and daughter nuclei. Interestingly, however, for

the description of many of the hitherto published $Z \geq 113$ decay chains it appears to suffice with just one type of decay sequence – i.e. that the decay of each isotope always proceeds with the same decay mode and from the same state – be it $^{287–289}115$ [12] or $^{293,294}117$ [13,14] (see also references therein). This simple but surprising picture might be due to limited statistics, combined with possibly comparable decay energies and half lives of different decay branches of a given isotope.

In Ref. [12] element 115 chains have been grouped partly according to their length. The observed four two-$\alpha$-long chains were observed at low excitation energy and were assigned to the isotope $^{289}115$, while all five-$\alpha$-long chains seen at the same excitation energy were assigned to the isotope $^{288}115$. However, in three of the four chains the observed decay times are very similar to the ones in the long chains. This suggests that those chains might actually originate from the isotope $^{288}115$, which would then imply the presence of a fission branch in the grand daughter of $^{288}115$.

In this paper, new data on seven short chains stemming from element $Z = 115$ are presented. The decay characteristics of all seven new chains essentially agree with the ones from the currently available data set of five-$\alpha$-long chains assigned to $^{288}115$. Five of these new chains are of recoil-$\alpha$–$\alpha$-SF type and two are of recoil-$\alpha$-SF type. The data from the Berkeley gas-filled separator, presented in Ref. [8], contain three short chains: one of recoil-$\alpha$–$\alpha$-SF type, and two of recoil-$\alpha$-SF type. Regardless of the exact isotope assignments, these data suggest that the plain length of an $\alpha$-decay chain is not necessarily a good descriptor to define the reaction channel, and that more complex decay sequences of $^{288,289}115$ than presented in previous reports on these isotopes [11,12,16] may be present. Here, alternative interpretations are proposed.

## 2. Experimental

The Universal Linear Accelerator (UNILAC) at the GSI Helmholtzzentrum für Schwerionenforschung, Darmstadt, Germany, provided a $^{48}Ca^{10+}$ heavy-ion beam with a typical intensity of $6 \times 10^{12}$ ions per second, averaged over the pulsed structure of the UNILAC (5 ms beam on and 15 ms beam off). The experiment was conducted at two beam energies. Beam integrals of 2.13(12) and 3.89(23) $\times 10^{18}$ $^{48}$Ca ions were collected at 5.400 and 5.462 MeV/u, respectively.

At the entrance of the recoil separator TASCA [17–19] the beam particles hit one out of four target segments, which were mounted on a rotating target wheel [20]. The thicknesses of these segments averaged to 0.83(1) mg/cm$^2$ $^{243}Am_2O_3$. The $^{243}$Am material originated from the Oak Ridge National Laboratory. At Mainz University the $^{243}$Am was electroplated onto 2.20(5) μm thick titanium backing foils [21]. The $^{48}$Ca beam first passed through these foils. Estimates for the energy-loss of $^{48}$Ca ions in titanium and $^{243}Am_2O_3$ lead to mid-target beam energies of 242.1 and 245.0 MeV [22]. Based on the Myers–Swiatecki mass table [23], these laboratory energies convert into compound nucleus excitation energies of $E^* = 32.4–37.9$ MeV and 34.8–40.3 MeV across the target layers.

TASCA, filled with He-gas at $p_{He} = 0.8$ mbar [24], was used in its so-called high-transmission mode [18] and set to centre ions with a magnetic rigidity of $B\rho = 2.21$ Tm in the focal plane for the major part of the experiment [25]. The multi-coincidence spectroscopy set-up TASISpec [26] was placed in TASCA's focal plane. The efficiency for transmitting element $Z = 115$ fusion-evaporation residues through TASCA and into TASISpec amounts to 30(3)% [25,27].

Five $32 \times 32$-strip Double-Sided Silicon Strip Detectors (DSSSD) form the heart of TASISpec. The ions passing through TASCA are implanted in one of 1024 pixels of the downstream DSSSD,

which is $6 \times 6$ cm$^2$ in area and 0.52 mm thick. Four additional DSSSDs with the same area but with thicknesses of 1.0 mm are placed upstream. They are sensitive to charged-particle decay radiation emitted from the implanted ions into the backward hemisphere. Detector strips of these four DSSSDs were paired together electrically, i.e., these DSSSDs are handled effectively as $16 \times 16$-strip detectors giving rise to another 1024 pixels. To detect photons coincident with charged-particle decays registered by the DSSSDs, five large, composite germanium detectors were placed closely around the box of silicon detectors, one behind each of the five DSSSDs [26].

The 96 preamplified signals [28] from the $n$-doped sides of the DSSSDs were recorded based on standard analog electronics [26]. The preamplified signals of the $p$-doped sides were digitized as 70-μs long traces by 60 MHz, 12-bit sampling ADCs [29]. The signals of the germanium detectors were handled by commercial 100-MHz, 16-bit sampling ADCs. The data acquisition was triggered by a coincident signal from a $p$-side and an $n$-side strip of the implantation detector. The latter limits the energy threshold of the trigger to some 0.4 MeV deposited. Since the experimental setup does not employ any MWPC veto detector upstream of the implantation detector – in contrast to other similar set-ups – the element 115 ions are implanted on average about 5 μm into the active detector volume. Therefore, even $\alpha$ particles that are emitted out of the implantation detector leave detectable amounts of energy in the active volume. The probability that an $\alpha$ particle of approximately 10 MeV deposits more energy in the implantation detector than the threshold value is estimated to $(97 \pm 2)\%$, i.e. the risk of missing an $\alpha$ decay completely is small.

Time-averaged (cf. pulsed UNILAC beam structure) trigger rates were typically 100–120 events per second. Beam on-off status and irradiated target segment number were recorded. The data acquisition system also provided the possibility to send a signal to the UNILAC control system to switch off the primary $^{48}$Ca beam upon detection of an 8.5–11.0-MeV particle in one of the $n$-side strips of the implantation DSSSD during UNILAC beam-off periods. The beam was then chopped within 20 μs for periods of 5–60 seconds (see Ref. [7]).

Si- and Ge-detector calibrations were performed using various radioactive sources in conjunction with precision pulser signals. During the offline data analysis, the calibrations were cross-checked with known $\alpha$-decay as well as $\gamma$-ray energies of background radiation mainly from transfer reaction products reaching the TASISpec implantation detector. More details on the detector set-up, electronics, data storage, and data analysis can be found in Refs. [7, 30–33].

As outlined in Ref. [7], a search for time- and position-correlated recoil-$\alpha$–$\alpha$, recoil-$\alpha$-SF, and recoil-SF sequences was conducted using

- $11.5 < E_{\mathrm{rec}} < 18.0$ MeV, beam on;
- $9.0 < E_{\alpha 1} < 12.0$ MeV, $\Delta t_{\mathrm{rec}-\alpha 1} = 5$ s, beam off, or
  $10.0 < E_{\alpha 1} < 12.0$ MeV, $\Delta t_{\mathrm{rec}-\alpha 1} = 1$ s, beam on;
- $9.0 < E_{\alpha 2} < 11.0$ MeV, $\Delta t_{\alpha 1-\alpha 2} = 20$ s, beam off, or
  $9.5 < E_{\alpha 2} < 11.0$ MeV, $\Delta t_{m\alpha 1-\alpha 2} = 5$ s, beam on;
- $E_{\mathrm{SF}} > 120$ MeV, $\Delta t_{\alpha 1-\mathrm{SF}} = 30$ s or $\Delta t_{\mathrm{rec}-\mathrm{SF}} = 30$ s, beam off.

Time and energy criteria for the search during beam-on periods are more restrictive than the ones for beam-off periods, in order to discriminate the random correlations that would otherwise result from the higher beam-on background rates. During beam-off and background measurement periods, only 64 fission events were recorded in total. Most of these were correlated with one of

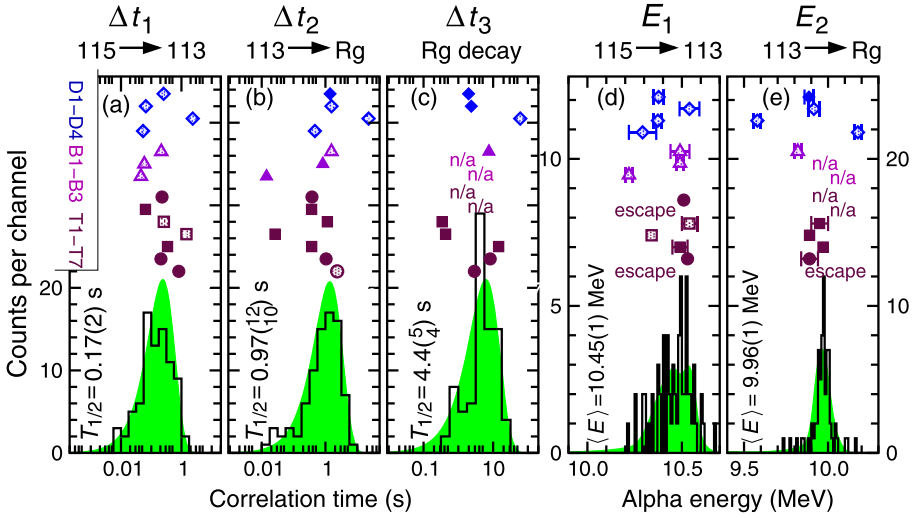


Fig. 1. (Colour online) Correlation times [(a)–(c)] and $\alpha$-energy spectra [(d) and (e)] of decay chains observed in the reaction $^{48}$Ca + $^{243}$Am. The term "$\alpha$ energy" includes possible summation with energy deposited by conversion or Auger electrons. The black histograms are reference spectra and relate to experimental data from the 96 chains associated with the 3$n$ evaporation channel $^{288}$115 in Refs. [7,8,12]. The shaded areas in panels (a)–(c) are the corresponding time distributions. The shaded areas in panels (d) and (e) are the energy distributions derived from Monte Carlo simulations as outlined in Refs. [7,32,35]. The data points of the fourteen observed recoil-$\alpha$–($\alpha$-)fission events are provided on top of each spectrum, labelled with an identifier according to Table 1. Filled symbols indicate measurement during beam-off periods. Diamonds refer to data from Ref. [12], triangles refer to data from Ref. [8], and squares and circles refer to the present data observed at 242.1 and 245.0 MeV mid-target beam energy, respectively. 'n/a' means 'not applicable', 'escape' denotes events with low-energy detection solely in the implantation DSSSD.

the thirty $\alpha$-decay chains, or could be associated with short-lived recoil-SF events of transfer reaction products such as $^{242m}$Am.

## 3. Results and compilation of data

The thirty identified chains associated with the production of element 115 contain 23 five-$\alpha$ long chains. The spectroscopic results on these have been communicated in Ref. [7], further described in Refs. [31,32], and are to be detailed in a forthcoming publication [33]. One of those 23 long chains was assigned to originate from the isotope $^{287}$115 and 22 from $^{288}$115 [7]. The combined data on the three first decay steps of these 22 decay chains, 31 corresponding ones from Ref. [12], and 43 from Ref. [8] are shown in Fig. 1. The black histograms are the experimental spectra. In panels (a)–(c), the number of correlation times available to derive the half-life, $T_{1/2}$, of a given decay step is 84, 83, and 84, respectively. Correlation times which follow upon a missing $\alpha$, or relate to $\alpha$-decays with tentative assignments, have been excluded. The expected time distributions for the corresponding half-lives are indicated by the shaded areas. In Figs. 1(d) and 1(e) the shaded areas relate to Geant4 Monte-Carlo simulations [34,35], which are based on decay schemes suggested in Refs. [7,31,32,35,36]. In short, one or several $\alpha$ decays populate excited states in the daughter nucleus. The excited states often decay via internal conversion. Energy summing of a detected $\alpha$ particle and one or more registered conversion or Auger electrons readily explains the relatively broad energy distributions observed. Energies given in tables

Table 1
Mid-target laboratory-frame beam energies, energies of the implanted recoils $E_{\rm rec}$, $\alpha$ energies $E_1$, $E_2$ and $E_3$, together with the associated correlation times of recoil-$\alpha$-SF and recoil-$\alpha$–$\alpha$-SF decay chains observed in the $^{48}$Ca + $^{243}$Am reaction. Entries in bold were recorded during beam-off periods. The number of $\gamma$ rays detected in prompt coincidence with SF events, $N_\gamma$(SF), is also specified. $N_{\rm random}$ corresponds to the number of chains of a given type expected to arise from random background [37]. The decay characteristics of the four chains listed in Table III in Ref. [12], denoted D1–D4, are included for completeness, as well as the recoil-$\alpha$(–$\alpha$)-SF chains listed in Supp. Mat. Table 2 in Ref. [8] denoted B1–B3. Uncertainties in decay energies are given as $\sigma_E$.

| No. | $\langle E_{\rm lab}\rangle$ (MeV) | $E_{\rm rec}$ (MeV) pixel ($x$, $y$) | $E_1$ (MeV) $\Delta t_1$ (s) | $E_2$ (MeV) $\Delta t_2$ (s) | $E_3$ (MeV) $\Delta t_3$ (s) | $N_\gamma$(SF) | $N_{\rm random}$ |
|---|---|---|---|---|---|---|---|
| T1 | 245.0 | 12.3 | **10.51(1)** | **242**[a] | | **6** | $<2\cdot10^{-5}$ |
| | | 268 (8, 12) | **0.227** | **0.378** | | | |
| T2 | 242.1 | 16.2 | **1.45(1)**[b] | **211** | | **>4** | $<6\cdot10^{-2}$ |
| | | 425 (13, 9) | **0.0645** | **0.366** | | | |
| T3 | 242.1 | 13.9 | 10.54(4)[c] | **9.95(5)**[c] | **196** | **8** | $<2\cdot10^{-6}$ |
| | | 681 (21, 9) | 0.261 | **1.15** | **0.343** | | |
| T4 | 242.1 | 14.5 | 10.34(1) | **9.89(1)** | **218**[a] | **>5** | $<2\cdot10^{-6}$ |
| | | 344 (10, 24) | 1.46 | **0.0262** | **0.432** | | |
| T5 | 242.1 | 13.8 | **10.49(4)**[c] | **9.97(1)** | **135** | **9** | $<3\cdot10^{-9}$ |
| | | 554 (17, 10) | **0.345** | **0.369** | **14.4** | | |
| T6 | 245.0 | 14.5 | **10.53(1)** | **9.89(5)**[c] | **230**[a] | **9** | $<3\cdot10^{-9}$ |
| | | 205 (6, 13) | **0.210** | **1.05** | **8.27** | | |
| T7 | 245.0 | 11.9 | **0.541(3)**[b] | 3.12(1)[b] | **230**[a] | **>4** | $<1\cdot10^{-1}$ |
| | | 128 (4, 0) | **0.815** | 2.33 | **2.89** | | |
| D1 | 240.5 | 11.38 | 10.377(26) | **9.886(26)** | **215.7** | | |
| | | | 0.2562 | **1.4027** | **1.9775** | | |
| D2 | 241.0 | 15.18 | 10.540(52)[c] | 9.916(31) | **214.9**[a] | | |
| | | | 0.0661 | 1.5500 | **2.3638** | | |
| D3 | 241.0 | 9.04 | 10.373(21) | 9.579(21) | 141.1 | | |
| | | | 2.3507 | 22.5822 | 60.1855 | | |
| D4 | 241.0 | 13.35 | 10.292(72)[c] | 10.178(23) | **182.2**[a] | | |
| | | | 0.0536 | 0.4671 | **0.0908** | | |
| B1 | 242 | 11.65 | 10.49(5) | 9.82(2) | **107** | **6** | |
| | | | 0.214 | 1.54 | **7.57** | | |
| B2 | 242 | 11.18 | 10.49(2) | **187**[a] | | **5** | |
| | | | 0.0591 | **0.824** | | | |
| B3 | 242 | 13.72 | 10.22(2) | **128** | | **2** | |
| | | | 0.0455 | **0.0142** | | | |

[a] Fission event registered by both implantation and box detector.
[b] Escaped $\alpha$ particle registered solely by the implantation detector.
[c] Reconstructed energy of an $\alpha$ particle registered by both implantation and box detector.

and figures always refer to the sum of $\alpha$ and electron energies, but will generally be called "$\alpha$ energies".

The experimental results from the present work consist of two recoil-$\alpha$-SF chains (denoted T1, T2) and five recoil-$\alpha$–$\alpha$-SF chains (T3–T7). These are summarized in Table 1, together with the four recoil-$\alpha$–$\alpha$-SF chains published by Oganessian et al. (D1–D4) [12] and the three recoil-$\alpha$(-$\alpha$)-SF chains published by Gates et al. [8] (B1–B3). The individual correlation times and $\alpha$ energies of the fourteen recoil-$\alpha$–($\alpha$)-SF chains are also shown in Fig. 1(a)–(e), labelled with T1–T7, D1–D4, and B1–B3, respectively. These fourteen chains will be referred to as "short chains".

The number of chains of a given type expected to arise from random background in the whole implantation DSSSD, $N_{\text{random}}$, has been calculated for the seven new chains according to Ref. [37]. The probability for one or more events of certain types to occur within predefined time periods are calculated assuming Poisson distributions. Here, escape events relate to energies up to 4 MeV in a DSSSD pixel, while 9–11 MeV is set for full energy and reconstructed events. Fission events are defined as beam-off events with more than 120 MeV detected. The number of fissions in a pixel is set to the actual number if this value is above zero, and to the average value over the implantation detector if the pixel contained no fission event. Time periods used in the calculations are 2 s, 10 s, and 50 s for decay steps one, two, and three, respectively. Count rates per pixel are determined in the two predefined energy ranges separately for beam-on and beam-off periods. Essentially, the non-random origins of TASISpec chains T1–T7 are defined by the overall small number of in total only 64 fission events observed during beam-off periods, in combination with the rather short time periods, $\Delta t$, between the detected recoil implantation and subsequent fission events. Nonetheless, for chains T2 and T7 approximately 0.1 random chains of each type are expected during the experiment.

It could be argued that the decay data suggested to originate from $^{293}117$ [9,11,13,38] could be included in this study. However, such data is deliberately not considered here. Presence of links between decay chains associated with elements 115 and 117 are neither questioned nor are they the subject of the present work. These issues deserve a dedicated study.

## 4. Statistical assessments

To assess whether distributions of experimental correlation times are compatible with the assumption that each step can be described by one single half-life, a relatively "new test for random events of an exponential distribution" [39] was applied to the 96 five-$\alpha$ long chains associated with the isotope $^{288}115$. In short, the method relies on the fact that the standard deviation $\sigma_\theta$ for a distribution of logarithms of lifetimes, $\theta = \ln(t)$, has a fixed value if the lifetimes originate from an exponential decay, however dependent on the number of available lifetimes. The 90% confidence intervals $[\sigma_{\theta,\text{low}}, \sigma_{\theta,\text{high}}]$ have been calculated for different number of data points by Monte Carlo techniques in Ref. [39]. A small value of $\sigma_\theta$ suggest that the lifetimes do not originate from an exponential distribution, and a large value indicates that decays from more than one species are present. The test is applied to (*i*) the full data set, and (*ii*) subdivisions into seven data sets corresponding to the seven different $^{48}$Ca beam energies employed in Refs. [7,8,12]. The result of this test can be found in Table 2. There is no clear hint towards the need of assuming the decay of more than one radioactive species for any of the decay steps of these 96 chains, thereby concurring with previous interpretations [12,31,32]. Therefore, and this is the most relevant result in the context of the present work, they serve as reference for the 3*n* evaporation channel $^{288}115$.

The focus lies now on the interpretation of the fourteen short chains. At first glance (see Fig. 1), there seems to be very little if any difference in the distribution of these data points compared with the distributions of the 96 five-$\alpha$ long chains associated with $^{288}115$. Interestingly, none of the early publications on decay chains associated with element 115 [12,31,32] dwell on this similarity. Instead, it has essentially been argued that the length of a decay chain is a sufficient descriptor of its origin: All five-$\alpha$ long chains observed at low excitation energies of the compound nucleus $^{291}115$, $E^* \lesssim 37$ MeV, were associated with the decay of the 3*n* evaporation channel $^{288}115$. In turn, chains D1–D4 were interpreted to originate exclusively from the 2*n* evaporation channel $^{289}115$, motivated by the non-observation of short chains at excitation

Table 2
Overview of analyses according to Ref. [39] of 96 five-$\alpha$ chains associated with $^{288}115$ at different beam energies [7,8,12]. $\sigma_{\Theta_{\mathrm{exp}}}$ refers to the standard deviation of the logarithms of lifetimes, and $[\sigma_{\Theta,\mathrm{low}}, \sigma_{\Theta,\mathrm{high}}]$ is the corresponding 90% confidence interval for the standard deviation. The letter **H** (**L**) highlights that $\sigma_{\Theta_{\mathrm{exp}}}$ is outside the respective 90% confidence interval on the high (low) side.

| $\langle E_{\mathrm{lab}} \rangle$ (MeV) | 239.8 | 240.8 | 242.1 | 243.4 | 245.0 | 248.1 | 242 | ALL |
|---|---|---|---|---|---|---|---|---|
| $E^*$ [23] | 31.1–35.3 | 31.4–36.4 | 32.4–37.9 | 34.0–38.3 | 34.8–40.3 | 38.0–42.3 | 36 | |
| $d_{\mathrm{target}}$ (mg/cm$^2$) | 0.37 | 0.84; 0.68 | 0.83(1) | 0.37 | 0.83(1) | 0.36; 0.37 | 0.54 | |
| Integral ($10^{18}$) | 11.7 | 10.4 | 2.13(12) | 3.3 | 3.89(23) | $4.3 + 3.7$ | | |
| No. of chains | 7 | 12 | 8 | 6 | 14 | $3 + 3$ | 43 | 96 |
| $\sigma_{\mathrm{prod}}$ (pb) | $3.5(^{27}_{15})$ | | $7.5(10)(^{36}_{26})$ | $8.5(^{64}_{37})$ | $7.2(9)(^{24}_{19})$ | $\sim$4 | | |
| $T_{1/2}(^{288}115)$ (s) | $0.14(^{10}_{4})$ | $0.18(^{8}_{4})$ | $0.24(^{15}_{7})$ | $0.15(^{12}_{5})$ | $0.10(^{4}_{2})$ | $0.18(^{13}_{5})$ | $0.18(^{4}_{3})$ | 0.17(2) |
| Data points; $\sigma_{\Theta_{\mathrm{exp}}}$ | 6; 1.70 | 10; 1.20 | 7; 0.72 | 5; 0.98 | 14; 0.72 **L** | 6; 1.20 | 37; 1.63 **H** | 84; 1.41 |
| $[\sigma_{\Theta,\mathrm{low}}, \sigma_{\Theta,\mathrm{high}}]$ | [0.48, 1.89] | [0.65, 1.82] | [0.52, 1.87] | [0.41, 1.90] | [0.73, 1.77] | [0.48, 1.89] | [0.93, 1.61] | [1.04, 1.51] |
| $T_{1/2}(^{284}113)$ (s) | $1.17(^{80}_{34})$ | $1.18(^{59}_{30})$ | $1.06(^{64}_{29})$ | $1.13(^{91}_{35})$ | $0.67(^{26}_{14})$ | $0.56(^{39}_{16})$ | $1.03(^{20}_{15})$ | $0.97(^{12}_{10})$ |
| Data points; $\sigma_{\Theta_{\mathrm{exp}}}$ | 6; 1.93 **H** | 9; 0.78 | 7; 0.78 | 5; 1.56 | 13; 0.99 | 6; 0.53 | 37; 1.58 | 83; 1.37 |
| $[\sigma_{\Theta,\mathrm{low}}, \sigma_{\Theta,\mathrm{high}}]$ | [0.48, 1.89] | [0.62, 1.84] | [0.52, 1.87] | [0.41, 1.90] | [0.72, 1.77] | [0.48, 1.89] | [0.93, 1.61] | [1.04, 1.51] |
| $T_{1/2}$ ($^{280}$Rg) (s) | $2.2(^{14}_{6})$ | $4.9(^{21}_{11})$ | $11.3(^{78}_{33})$ | $3.9(^{27}_{11})$ | $4.0(^{17}_{9})$ | $4.2(^{29}_{12})$ | $3.9(^{8}_{5})$ | $4.4(^{5}_{4})$ |
| Data points; $\sigma_{\Theta_{\mathrm{exp}}}$ | 7; 0.88 | 11; 1.11 | 6; 0.40 **L** | 6; 0.94 | 11; 1.04 | 6; 0.84 | 37; 0.73 **L** | 84; 0.932 **L** |
| $[\sigma_{\Theta,\mathrm{low}}, \sigma_{\Theta,\mathrm{high}}]$ | [0.52, 1.87] | [0.67, 1.81] | [0.48, 1.89] | [0.48, 1.89] | [0.67, 1.81] | [0.48, 1.89] | [0.93, 1.61] | [1.04, 1.51] |
| $T_{1/2}$ ($^{276}$Mt) (s) | $0.90(^{55}_{25})$ | $0.53(^{26}_{13})$ | $1.5(^{12}_{5})$ | $0.29(^{29}_{10})$ | $0.42(^{18}_{10})$ | $0.90(^{73}_{28})$ | $0.67(^{13}_{10})$ | $0.69(^{9}_{7})$ |
| Data points; $\sigma_{\Theta_{\mathrm{exp}}}$ | 7; 1.25 | 9; 1.14 | 5; 1.62 | 4; 1.21 | 11; 0.62 **L** | 5; 0.88 | 36; 1.36 | 77; 1.25 |
| $[\sigma_{\Theta,\mathrm{low}}, \sigma_{\Theta,\mathrm{high}}]$ | [0.52, 1.87] | [0.62, 1.84] | [0.41, 1.90] | [0.31, 1.92] | [0.67, 1.81] | [0.41, 1.90] | [0.92, 1.62] | [1.03, 1.52] |
| $T_{1/2}$ ($^{272}$Bh) (s) | $4.1(^{25}_{11})$ | $24(^{16}_{67})$ | $9.7(^{67}_{28})$ | $6.4(^{64}_{21})$ | $9.0(^{42}_{22})$ | $14(^{11}_{4})$ | $10.2(^{23}_{16})$ | $10.5(^{15}_{11})$ |
| Data points; $\sigma_{\Theta_{\mathrm{exp}}}$ | 7; 1.51 | 6; 1.30 | 6; 0.76 | 4; 1.59 | 10; 1.12 | 5; 0.86 | 29; 1.22 | 67; 1.32 |
| $[\sigma_{\Theta,\mathrm{low}}, \sigma_{\Theta,\mathrm{high}}]$ | [0.52, 1.87] | [0.48, 1.89] | [0.48, 1.89] | [0.31, 1.92] | [0.65, 1.82] | [0.41, 1.90] | [0.88, 1.65] | [1.01, 1.53] |
| $T_{1/2}$ ($^{268}$Db) (h) | $23(^{14}_{6})$ | $15(^{6}_{3})$ | $22(^{12}_{6})$ | $34(^{23}_{10})$ | $28(^{10}_{6})$ | $34(^{23}_{10})$ | $32(^{7}_{5})$ | 28(3) |
| Data points; $\sigma_{\Theta_{\mathrm{exp}}}$ | 7; 0.77 | 12; 0.83 | 8; 1.04 | 6; 0.89 | 14; 1.20 | 6; 0.73 | 31; 1.00 | 84; 1.01 **L** |
| $[\sigma_{\Theta,\mathrm{low}}, \sigma_{\Theta,\mathrm{high}}]$ | [0.52, 1.87] | [0.70, 1.79] | [0.58, 1.85] | [0.48, 1.89] | [0.73, 1.77] | [0.48, 1.89] | [0.90, 1.64] | [1.04, 1.51] |

Table 3
Half-lives derived from the correlation times of decays of isotopes of Rg, $Z = 113$ and $Z = 115$. Results and confidence intervals of a statistical test proposed in Ref. [39] are provided for each half-life analysis. The four columns describe different combinations of the decay data from recoil-$\alpha$-SF and recoil-$\alpha$–$\alpha$-SF events detailed in Table 1, and data related to the $3n$ reaction channel in Refs. [7,8,12,31]. $\sigma_{\Theta_{\text{exp}}}$ refers to the standard deviation of the logarithms of lifetimes, and $[\sigma_{\Theta,\text{low}}, \sigma_{\Theta,\text{high}}]$ is the corresponding 90% confidence interval for the standard deviation. The letter **H** (**L**) highlights that $\sigma_{\Theta_{\text{exp}}}$ is outside the respective 90% confidence interval on the high (low) side.

| Data selection | T1–T7 D1–D4 B1–B3 | T1–T7 D1, D2, D4 B1–B3 | $3n$, T1–T7 D1–D4 B1–B3 | $3n$, T1–T7 D1, D2, D4 B1–B3 |
|---|---|---|---|---|
| $T_{1/2}(Z = 115)$ (s) | $0.32(^{12}_{7})$ | $0.217(^{83}_{47})$ | $0.191(^{21}_{18})$ | $0.177(^{20}_{16})$ |
| Data points; $\sigma_{\Theta_{\text{exp}}}$ | 14; 1.20 | 13; 1.04 | 98; 1.39 | 97; 1.37 |
| $[\sigma_{\Theta,\text{low}}, \sigma_{\Theta,\text{high}}]$ [39] | [0.73, 1.77] | [0.72, 1.77] | [1.06, 1.49] | [1.06, 1.49] |
| $T_{1/2}(Z = 113)$ (s) | $1.69(^{61}_{36})$ | $0.61(^{24}_{13})$ | $1.08(^{12}_{10})$ | $0.92(^{11}_{9})$ |
| Data points; $\sigma_{\Theta_{\text{exp}}}$ | 14; 1.75 | 13; 1.50 | 97; 1.43 | 96; 1.40 |
| $[\sigma_{\Theta,\text{low}}, \sigma_{\Theta,\text{high}}]$ [39] | [0.73, 1.77] | [0.72, 1.77] | [1.06, 1.49] | [1.06, 1.49] |
| $T_{1/2}$ (Rg) (s) | $6.8(^{32}_{16})$ | $3.0(^{15}_{7})$ | $4.67(^{54}_{44})$ | $4.27(^{49}_{40})$ |
| Data points; $\sigma_{\Theta_{\text{exp}}}$ | 10; 1.84 **H** | 9; 1.59 | 94; 1.08 | 93; 1.05 |
| $[\sigma_{\Theta,\text{low}}, \sigma_{\Theta,\text{high}}]$ [39] | [0.65, 1.82] | [0.62, 1.84] | [1.05, 1.50] | [1.05, 1.50] |

energies $\gtrsim$ 36 MeV [12]. However, the non-observation of short chains could be due to a lack of statistics or difficulties to detect short chains using continuous-beam experiments such as, e.g., in Refs. [9–13]. For short chains in particular, the detection of fission during clean conditions is crucial to establish the non-randomness of a chain. For continuous-beam experiments, this requires that an $\alpha$ triggers a beam shut-off.

The interpretation that all short chains originate from $^{289}115$ provides one explanation of the data. The $\sigma_\theta$ values for the three decay steps in the set of fourteen short chains are 1.20, 1.75, 1.84, and should be compared with the intervals [0.73, 1.77], [0.73, 1.77], and [0.65, 1.82], respectively (see column 2 in Table 3). All but the last step fit within the intervals. The similarities between the short chains and the 96 decay chains from $^{288}115$ suggest another possibility. Adding the short chains to this data set, giving a total of 110 chains, yields $\sigma_\theta$ values [39] of 1.39, 1.43, and 1.08 for the first three decay steps containing 98, 97, and 94 data points, respectively. All three fall within the respective 90% confidence intervals [1.06, 1.49], [1.06, 1.49], and [1.05–1.50] (see column 4 in Table 3). This gives a first indication that the 110 chains could form a set in which all members follow the same decay sequence.

Another aspect, which has not been discussed previously, is the fact that the D3 chain looks different compared to all other chains. A closer inspection of Fig. 1 suggests that chain D3 is compatible neither with the $3n$ reference values nor the average of the remaining thirteen recoil-$\alpha$–($\alpha$)-SF events: all of the three decay times of D3 are approximately ten times larger than the respective reference time distribution. The reported $\alpha$ energy $E_2$ is also significantly lower than that of the remaining short chains where the full energy was measured. While a single extreme value would not pose a statistical problem, the fact that in chain D3 four out of five observables differ significantly from the expectations does. The test devised in Ref. [39] applies to only one decay step at the time, but not to *chains*. Hence, the non-characteristic decay data of the whole D3 chain could be interesting to look at in more detail. In column 3 of Table 3, the $\sigma_\theta$ values for the set of short chains where D3 is excluded are presented: All values are now within the respective interval.

Table 4
FoM$_j$ and FoM$_{geom}$ for each of the short decay chains, and FoM for the entire set of fourteen chains when they are compared with a reference formed by the chains themselves (see text for details).

| Chain ID | FoM$_1$ | FoM$_2$ | FoM$_3$ | FoM$_{geom}$ |
|---|---|---|---|---|
| T1 | 0.282 | 0.124 | n/a | 0.187 |
| T2 | 0.113 | 0.120 | n/a | 0.117 |
| T3 | 0.302 | 0.276 | 0.030 | 0.136 |
| T4 | 0.168 | 0.010 | 0.038 | 0.040 |
| T5 | 0.336 | 0.121 | 0.336 | 0.239 |
| T6 | 0.271 | 0.262 | 0.337 | 0.288 |
| T7 | 0.310 | 0.352 | 0.198 | 0.278 |
| D1 | 0.300 | 0.304 | 0.148 | 0.238 |
| D2 | 0.116 | 0.317 | 0.170 | 0.184 |
| D3 | 0.061 | 0.007 | 0.047 | 0.027 |
| D4 | 0.097 | 0.147 | 0.008 | 0.049 |
| B1 | 0.274 | 0.317 | 0.330 | 0.306 |
| B2 | 0.105 | 0.225 | n/a | 0.154 |
| B3 | 0.083 | 0.005 | n/a | 0.021 |
| FoM | | | | 0.162 |

The two observations – similarities between the short chains and $^{288}115$ chains, and the D3 chain's characteristics – are turned into a more robust figure-of-merit (FoM) as described in the appendix. Based on measured lifetimes, it provides a measure for the congruence of a set of *chains* with respect to itself or to an external 'reference' ensemble of chains. Deviations in $\alpha$ energy only serve as supportive argument, since the comprehensive data of element 115 decay chains suggests a range of energies rather than distinct peaks for decay steps $115 \rightarrow 113$ and $113 \rightarrow$ Rg [7,32,36]. The FoM method is applied to the data set consisting of $N = 14$ short chains – ten recoil-$\alpha$–$\alpha$-SF chains and four recoil-$\alpha$-SF chains – using themselves as a reference. The detailed results are presented in Table 4. The overall FoM is 0.162.

The FoM should, with 90% confidence, fall within the interval $[0.181, 0.255]$. The obtained FoM $= 0.162$ does not. Actually, this FoM is even outside the 98% confidence interval $[0.164, 0.269]$. Thus, the risk of being wrong is very small, when stating that the short chains do *not* constitute a set of chains that have the same origin and follow the same decay sequence, and that they should *not* be grouped together. Considering FoM$_{geom}$ for individual chains (see Table 4), it can also be noted that chains D3, D4, T4, and B3, are all outside their respective 90% confidence intervals, which have lower limits of 0.080 and 0.064 for recoil-$\alpha$–$\alpha$-SF and recoil-$\alpha$-SF chains, respectively (see Fig. 6).

To examine the data set of fourteen short chains in more detail, each chain was excluded one at a time, and then the FoM of the remaining thirteen chains were examined. The FoM are listed in the second column of Table 5. Since the new data sets contain only thirteen chains and have either nine or ten members in the last step, they have slightly different confidence intervals. The *only* way to exclude only one chain and obtain a FoM within the 90% confidence interval is to exclude chain D3. Very likely, this chain has a decay sequence different from all other thirteen short chains. The third column of Table 5 shows FoM$_{geom}$ for the excluded chain when compared with the external reference formed by the remaining thirteen chains. Also here, D3 has a remarkably low value. Other chains that agree less well with the remaining chains are D4, T4 and B3.

Table 5
In the first row, FoM and half-lives $T^i_{1/2}$ for decay steps $i = 1, 2, 3$ for the set of fourteen short chains are presented. In the following rows, one chain at the time is excluded from the set of fourteen chains. The second column relate to the FoM for the set of thirteen remaining short chains. FoM for sets where a recoil-$\alpha$–$\alpha$-SF chain is excluded should be in the confidence interval [0.178, 0.256]. The FoM indexed with * (a recoil-$\alpha$-SF chain is excluded) should be in the confidence interval [0.179, 0.255]. The third column shows $\mathrm{FoM}_{geom}$ for the *excluded chain* when its characteristics is compared with the external reference formed by the remaining thirteen chains. Columns four, five, and six, are the half-lives $T^j_{1/2}$ for decay steps $i = 1, 2, 3$ for the respective set of thirteen chains. See text for more details.

| Chain ID | FoM | $\mathrm{FoM}_{geom}$ | $T^1_{1/2}$ (s) | $T^2_{1/2}$ (s) | $T^3_{1/2}$ (s) |
|---|---|---|---|---|---|
| ALL | 0.162 | – | 0.318 | 1.69 | 6.83 |
| T1 excl. | 0.157* | 0.179 | 0.331 | 1.80 | 6.83 |
| T2 excl. | 0.161* | 0.110 | 0.339 | 1.80 | 6.83 |
| T3 excl. | 0.159 | 0.129 | 0.329 | 1.75 | 7.56 |
| T4 excl. | 0.170 | 0.034 | 0.265 | 1.81 | 7.55 |
| T5 excl. | 0.154 | 0.232 | 0.324 | 1.80 | 6.48 |
| T6 excl. | 0.149 | 0.281 | 0.332 | 1.76 | 6.95 |
| T7 excl. | 0.153 | 0.269 | 0.299 | 1.69 | 7.37 |
| D1 excl. | 0.152 | 0.229 | 0.329 | 1.74 | 7.44 |
| D2 excl. | 0.156 | 0.175 | 0.339 | 1.73 | 7.41 |
| D3 excl. | 0.215 | 0.001 | 0.217 | 0.61 | 2.95 |
| D4 excl. | 0.164 | 0.045 | 0.340 | 1.79 | 7.58 |
| B1 excl. | 0.148 | 0.300 | 0.331 | 1.73 | 7.00 |
| B2 excl. | 0.159* | 0.146 | 0.340 | 1.77 | 6.83 |
| B3 excl. | 0.168* | 0.020 | 0.340 | 1.81 | 6.83 |

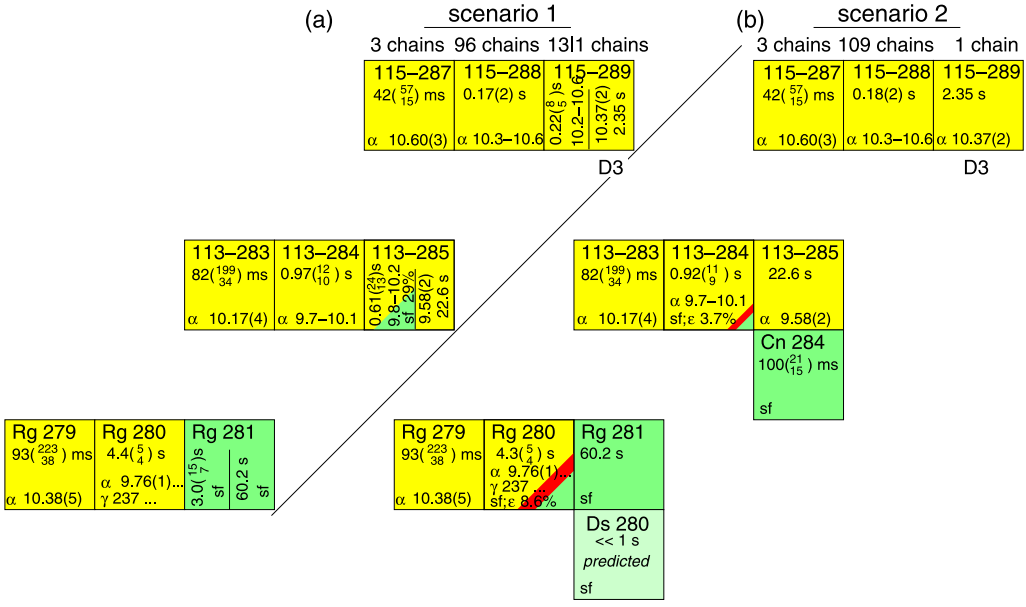


Fig. 2. (Colour online.) Two different decay scenarios of directly produced isotopes of element $Z = 115$ down to Rg, using previously published [7,8,12] and present data. Half-lives, $T_{1/2}$, are provided with uncertainties. Particle-decay energies or ranges of decay energies are given in MeV, $\gamma$-ray energies in keV. See text for detailed discussions.

Table 6
Number of chains and production cross sections, $\sigma_{\text{prod}}$, of $^{287-289}115$ derived for two decay scenarios (cf. Fig. 2) from the thirty decay chains observed in the TASISpec experiment (chains T1–T7 and 23 five-$\alpha$ long chains [7]). The observation of a single decay chain relates to a production cross section of $\sigma = 0.93(12)$ and 0.51(7) pb for mid-target beam energies 242.1 and 245.0 MeV, respectively. The systematic uncertainty accounts for uncertainties in beam integrals, target thickness, transport efficiency, and identification probability. Standard deviations of systematic uncertainties are given together with statistical uncertainties using a 68% confidence level [37].

| $\langle E_{\text{lab}} \rangle$ (MeV) | $E^*$ (MeV) [23] | Reaction channel | Scenario 1 | | Scenario 2 | |
|---|---|---|---|---|---|---|
| | | | No. of chains | $\sigma_{\text{prod}}$ (pb) | No. of chains | $\sigma_{\text{prod}}$ (pb) |
| 242.1 | 32.4–37.9 | 2$n$ | 4 | $3.7 \pm 0.5^{+2.8}_{-1.9}$ | 0 | $< 1.9$ |
| | | 3$n$ | 8 | $7.5 \pm 1.0^{+3.6}_{-2.6}$ | 12 | $11.2 \pm 1.4^{+4.2}_{-3.2}$ |
| | | 4$n$ | 0 | $< 1.9$ | 0 | $< 1.9$ |
| 245.0 | 34.8–40.3 | 2$n$ | 3 | $1.5 \pm 0.2^{+1.4}_{-0.9}$ | 0 | $< 1.1$ |
| | | 3$n$ | 14 | $7.2 \pm 0.9^{+2.4}_{-1.9}$ | 17 | $8.7 \pm 1.1^{+2.6}_{-2.1}$ |
| | | 4$n$ | 1 | $0.51 \pm 0.07^{+1.17}_{-0.42}$ | 1 | $0.51 \pm 0.07^{+1.17}_{-0.42}$ |

Columns four, five, and six, in Table 5 contain the resulting half-lives $T^j_{1/2}$ for decay steps $j = 1, 2, 3$ when one chain at the time is excluded. The exclusion of D3 changes the half-life considerably, while all other subsets have half-lives similar to the ones where the entire data set is considered. D3 obviously has a large impact on the half-life, posing another argument why D3 should not be grouped together with the other thirteen short chains.

Having examined the data set as above, it seems inevitable to assign chain D3 to another decay sequence than the other short chains. This leads to a change in the characteristics of element 115 isotopes in terms of half-lives, $\alpha$ energies and branching ratios, and a potential change in the isotope assignments. Two possible scenarios, where the D3 chain forms a separate decay sequence, are discussed below.

*Scenario 1*

In this scenario, the short chains are all assigned to the isotope $^{289}115$, with D3 forming a separate decay sequence. This interpretation is illustrated in "scenario 1" in Fig. 2(a). It can be noted that the decay times of D3 are similar to the chain $^{289}\text{Fl} \rightarrow {}^{285}\text{Cn} \rightarrow {}^{281}\text{Ds}$ [10,19,40]. This decay sequence can in principle be entered by EC decay of $^{289}115$ or $^{285}113$. However, both $\alpha$ energies measured for D3 differ distinctively from the ones expected for the mentioned even-$Z$ chain. Therefore, this explanation for D3 is disregarded. The remaining thirteen short chains that are assigned to the isotope $^{289}115$ in this scenario have half-lives $T^i_{1/2}$ for decay steps $i = 1, 2, 3$ that are very similar to the respective half-lives in the $^{288}115$ chains. The resulting cross sections are given in Table 6.

*Scenario 2*

In this scenario, D3 is tentatively left being the only chain starting from $^{289}115$, while the other thirteen chains are interpreted to start with $^{288}115$ and end with either SF or EC decay branches in $^{284}113$ or $^{280}\text{Rg}$. The $\sigma_\theta$ values for the set of 96 long chains and thirteen short chains are shown in column 5 in Table 3 together with the resulting half-lives.

In Table 7, the $\text{FoM}_{geom}$ have been calculated for each individual element 115 chain, with respect to the 96 chains assigned to $^{288}115$. In general, the short chains have $\text{FoM}_{geom}$ that are comparable with the $^{288}115$ chains, which supports this scenario. The extremely low $\text{FoM}_{geom}$

Table 7
Probability check of the first three decay steps of all 113 hitherto published decay chains (Refs. [7,8,12] and present data set) associated with the direct production of an isotope of element $Z = 115$. For each of the decay steps, $j = 1, 2, 3$ the $\mathrm{FoM}_j^{(n)}$ is given. Reference values are $T_{1/2}(Z = 115) = 0.17(2)$ s, $T_{1/2}(Z = 113) = 0.97(^{12}_{10})$ s, and $T_{1/2}(\mathrm{Rg}) = 4.4(^{5}_{4})$ s, corresponding to the 96 five-$\alpha$-long decay chains associated with the decay of $^{288}115$ (cf. Ref. [31,36] and Fig. 1). $\alpha$ energies are marked '+', 'L', 'H', if the measured energy is compatible with the range $E_1 = [10.3, 10.6]$ MeV and $E_2 = [9.7, 10.1]$ MeV or either too low or too high, respectively. These energy ranges are defined by full-energy measurements given in Ref. [12], and full- or reconstructed energy measurements provided in Refs. [7,8], cross-checked with Geant4 simulations [7,32,35,36]. An entry 'n/a' denotes incomplete or missing data.

| Chain ID | $\mathrm{FoM}_1$ | $\mathrm{FoM}_2$ | $\mathrm{FoM}_3$ | $\mathrm{FoM}_{geom}$ | $E_1$ | $E_2$ |
|---|---|---|---|---|---|---|
| Chains attributed to the $3n$ channel in Ref. [7] | | | | | | |
| 1 | 0.336 | 0.339 | 0.306 | 0.327 | + | L |
| 2 | 0.347 | 0.360 | n/a | 0.354 | + | + |
| 3[a] | n/a | n/a | 0.173 | 0.173 | n/a | + |
| 4 | 0.361 | 0.365 | 0.071 | 0.211 | + | + |
| 5 | 0.337 | 0.143 | 0.303 | 0.245 | + | + |
| 6 | 0.192 | 0.347 | n/a | 0.258 | n/a | + |
| 7 | 0.204 | 0.229 | 0.354 | 0.255 | + | + |
| 8 | 0.245 | 0.311 | 0.155 | 0.228 | n/a | + |
| 9 | 0.330 | 0.343 | n/a | 0.336 | + | + |
| 10 | 0.212 | 0.249 | 0.190 | 0.216 | n/a | + |
| 11 | 0.138 | 0.067 | 0.365 | 0.150 | + | + |
| 12 | 0.361 | 0.297 | 0.244 | 0.296 | + | + |
| 13[a] | 0.192 | 0.182 | 0.080 | 0.141 | n/a | + |
| 14 | 0.359 | 0.182 | n/a | 0.256 | + | + |
| 15 | 0.302 | 0.342 | 0.301 | 0.314 | + | + |
| 16 | 0.336 | 0.111 | 0.297 | 0.223 | + | L |
| 17 | 0.201 | 0.299 | 0.333 | 0.272 | n/a | + |
| 18 | n/a | 0.350 | 0.366 | 0.358 | n/a | + |
| 19 | 0.137 | 0.131 | 0.298 | 0.175 | + | + |
| 20 | 0.192 | 0.356 | 0.302 | 0.274 | + | + |
| 21 | 0.289 | n/a | n/a | 0.289 | + | n/a |
| 22 | 0.366 | 0.349 | 0.104 | 0.237 | n/a | + |
| Chains attributed to the $3n$ channel in Ref. [12] | | | | | | |
| 1 | n/a | n/a | 0.083 | 0.083 | n/a | + |
| 2 | 0.222 | 0.312 | 0.103 | 0.193 | + | + |
| 3[a] | 0.027 | 0.295 | 0.198 | 0.116 | + | + |
| 4 | 0.125 | 0.363 | 0.365 | 0.255 | + | + |
| 5[a] | 0.108 | 0.015 | 0.304 | 0.079 | + | + |
| 6[a] | 0.058 | 0.061 | 0.357 | 0.108 | + | + |
| 7[a] | 0.028 | 0.200 | 0.346 | 0.125 | + | + |
| 8 | 0.209 | 0.207 | 0.109 | 0.167 | + | + |
| 9[a] | 0.143 | 0.365 | 0.065 | 0.150 | + | + |
| 10 | 0.117 | 0.342 | 0.344 | 0.240 | + | + |
| 11 | n/a | n/a | 0.365 | 0.365 | n/a | + |
| 12 | n/a | n/a | 0.366 | 0.366 | n/a | + |
| 13 | 0.315 | 0.348 | 0.342 | 0.335 | + | + |
| 14[a] | 0.053 | 0.236 | 0.364 | 0.166 | + | + |
| 15[a] | 0.167 | 0.108 | 0.248 | 0.165 | + | + |
| 16 | 0.329 | 0.341 | 0.123 | 0.240 | + | + |

(*continued on next page*)

Table 7 (*Continued*)

| Chain ID | $\mathrm{FoM}_1$ | $\mathrm{FoM}_2$ | $\mathrm{FoM}_3$ | $\mathrm{FoM}_{geom}$ | $E_1$ | $E_2$ |
|---|---|---|---|---|---|---|
| 17 | 0.283 | 0.278 | 0.233 | 0.264 | + | + |
| 18 | 0.339 | n/a | n/a | 0.339 | + | n/a |
| 19 | 0.353 | 0.309 | 0.315 | 0.325 | + | + |
| 20 | 0.185 | 0.312 | 0.321 | 0.265 | + | + |
| 21[a] | 0.204 | 0.030 | 0.362 | 0.131 | + | + |
| 22 | 0.130 | 0.366 | 0.285 | 0.238 | + | + |
| 23[b] | 0.353 | 0.297 | 0.191 | 0.272 | + | + |
| 24[a] | 0.294 | 0.097 | 0.126 | 0.154 | + | + |
| 25 | n/a | n/a | 0.200 | 0.200 | n/a | + |
| 26 | 0.259 | 0.334 | 0.211 | 0.263 | + | + |
| 27 | 0.365 | 0.365 | 0.306 | 0.344 | + | + |
| 28 | 0.106 | 0.199 | 0.210 | 0.164 | + | + |
| 29 | 0.233 | 0.202 | 0.298 | 0.242 | + | + |
| 30 | 0.069 | 0.361 | 0.316 | 0.199 | + | + |
| 31 | 0.363 | 0.252 | 0.210 | 0.268 | + | + |
| Chains attributed to the 3*n* channel in Ref. [8] | | | | | | |
| 1 | 0.364 | 0.363 | 0.331 | 0.352 | L | + |
| 2 | 0.210 | 0.263 | 0.347 | 0.268 | + | + |
| 3 | 0.266 | 0.320 | 0.322 | 0.301 | H | + |
| 4 | 0.328 | 0.059 | n/a | 0.139 | + | + |
| 5 | 0.324 | 0.366 | 0.365 | 0.351 | + | + |
| 6 | 0.230 | 0.327 | 0.334 | 0.293 | n/a | + |
| 7 | 0.041 | 0.194 | 0.315 | 0.136 | n/a | + |
| 8 | 0.351 | 0.267 | 0.357 | 0.322 | + | + |
| 9 | 0.190 | 0.019 | 0.313 | 0.105 | + | + |
| 10 | 0.323 | 0.174 | 0.099 | 0.177 | L | + |
| 11 | 0.365 | n/a | n/a | 0.365 | n/a | n/a |
| 12 | 0.073 | 0.318 | 0.107 | 0.135 | n/a | + |
| 13 | 0.001 | 0.365 | 0.366 | 0.046 | n/a | + |
| 14 | n/a | 0.363 | 0.364 | 0.363 | L | + |
| 15 | 0.080 | 0.359 | 0.350 | 0.216 | L | + |
| 16 | 0.348 | 0.231 | 0.350 | 0.305 | + | H |
| 17 | 0.208 | 0.259 | 0.266 | 0.243 | n/a | + |
| 18 | 0.286 | 0.118 | n/a | 0.184 | + | + |
| 19 | 0.033 | 0.037 | 0.354 | 0.075 | + | + |
| 20 | 0.075 | 0.281 | 0.311 | 0.187 | + | + |
| 21 | 0.133 | 0.324 | 0.339 | 0.245 | + | + |
| 22 | 0.312 | 0.009 | 0.326 | 0.097 | + | + |
| 23 | 0.336 | 0.052 | 0.319 | 0.177 | L | + |
| 24 | 0.267 | 0.304 | 0.295 | 0.288 | + | + |
| 25 | 0.157 | 0.325 | 0.132 | 0.189 | + | + |
| 26 | 0.094 | 0.254 | 0.355 | 0.204 | + | + |
| 27 | 0.233 | 0.067 | 0.362 | 0.178 | + | + |
| 28 | 0.330 | 0.205 | 0.323 | 0.280 | + | + |
| 29 | n/a | 0.303 | 0.319 | 0.311 | + | + |
| 30 | 0.264 | 0.265 | 0.331 | 0.285 | + | + |
| 31 | 0.172 | 0.166 | 0.178 | 0.172 | + | + |
| 32 | 0.342 | 0.132 | 0.360 | 0.253 | + | + |
| 33 | 0.237 | 0.259 | 0.254 | 0.250 | n/a | + |
| 34 | 0.363 | 0.365 | 0.313 | 0.346 | + | + |

Table 7 (*Continued*)

| Chain ID | $\mathrm{FoM}_1$ | $\mathrm{FoM}_2$ | $\mathrm{FoM}_3$ | $\mathrm{FoM}_{geom}$ | $E_1$ | $E_2$ |
|---|---|---|---|---|---|---|
| 35 | 0.360 | 0.014 | 0.230 | 0.105 | + | + |
| 36 | 0.360 | n/a | n/a | 0.360 | + | n/a |
| 37 | n/a | n/a | 0.168 | 0.168 | n/a | + |
| 38 | 0.029 | 0.058 | 0.345 | 0.083 | H | + |
| 39 | 0.365 | 0.337 | n/a | 0.351 | + | + |
| 40 | 0.343 | 0.263 | 0.362 | 0.320 | + | n/a |
| 41 | n/a | n/a | n/a | 0.000 | n/a | n/a |
| 42 | n/a | n/a | 0.315 | 0.315 | n/a | H |
| 43 | n/a | n/a | 0.359 | 0.359 | n/a | n/a |
| Chains attributed to the 4*n* channel in Refs. [7,12] | | | | | | |
| 1 | 0.207 | 0.046 | 0.002 | 0.029 | H | H |
| 2 | 0.151 | n/a | n/a | 0.151 | + | n/a |
| 3 | 0.155 | 0.093 | 0.037 | 0.081 | + | H |
| Recoil-$\alpha$–($\alpha$)-SF chains, present data and Refs. [8,12] | | | | | | |
| T1 | 0.364 | 0.203 | n/a | 0.272 | + | n/a |
| T2 | 0.200 | 0.199 | n/a | 0.199 | n/a | n/a |
| T3 | 0.365 | 0.358 | 0.051 | 0.188 | + | + |
| T4 | 0.019 | 0.018 | 0.063 | 0.028 | + | + |
| T5 | 0.345 | 0.200 | 0.239 | 0.255 | + | + |
| T6 | 0.361 | 0.351 | 0.354 | 0.355 | + | + |
| T7 | 0.126 | 0.317 | 0.285 | 0.225 | n/a | n/a |
| D1 | 0.366 | 0.366 | 0.225 | 0.311 | + | + |
| D2 | 0.203 | 0.364 | 0.253 | 0.266 | + | + |
| D3 | 0.001 | 0.000 | 0.001 | 0.000 | + | L |
| D4 | 0.173 | 0.236 | 0.014 | 0.083 | + | H |
| B1 | 0.362 | 0.364 | 0.361 | 0.362 | + | + |
| B2 | 0.187 | 0.323 | n/a | 0.246 | + | n/a |
| B3 | 0.152 | 0.010 | n/a | 0.039 | L | n/a |

[a] Chain assignment relies also on $\alpha$ energies and correlation times of subsequent decay steps [33].
[b] The long-lived $\alpha$ decay assigned to $^{276}$Mt in Ref. [12] is associated with $^{280}$Rg [7].

of D3 supports its exclusion. A few other chains – T4, D4, and B3 – have rather low $\mathrm{FoM}_{geom}$, and their assignment to $^{288}115$ could be questioned.

This interpretation is illustrated in Fig. 2(b) as "scenario 2". This assignment of the thirteen chains to $^{288}115$ implies, at first sight, SF branching ratios of $b_{\mathrm{SF}} = 4/109 = 3.7\%$ for $^{284}113$ and $b_{\mathrm{SF}} = 9/105 = 8.6\%$ for $^{280}$Rg, respectively. It is important to note, however, that none of the experiments have been sensitive to EC decay. Hence, other options are EC decay branches of $^{284}113$ or $^{280}$Rg into even–even $^{284}$Cn or $^{280}$Ds. The latter are either known (see, e.g., Refs. [10,19,40]) or expected (see, e.g., Refs. [41–43]) to decay with $T_{1/2}(\mathrm{SF}) \ll 1$ s. In this scenario, partial SF or EC half-lives amount to about 30 s and 50 s for $^{284}113$ and $^{280}$Rg, respectively. This suggests that the respective SF hindrance factors are approximately 300 and 500 relative to $^{284}$Cn. These values are rather low for odd–odd nuclei, because hindrance is expected from each of the two unpaired nucleons. Already for one unpaired nucleon, hindrance factors are typically above 1000 [44,45]. Thus, we rather suggest EC preceding SF of the respective even–even daughter.

The observation of SF or EC branches in this region of the nuclear chart is consistent with recent theoretical estimates [46,47] (see especially Figs. 4 and 6 in Ref. [46]). For the half-life

analysis in Table 3, SF of $^{284}$113 and $^{280}$Rg has been assumed, i.e., the short finite lifetime of a potential EC daughter has not been considered.

*Further alternatives*

Guided by Schmidt's test [39] and the FoM values, two different scenarios have been suggested – one in which all short chains are assigned to start from $^{289}$115 (with D3 forming a separate decay sequence), and one in which all short chains except D3 start from $^{288}$115. Most likely, the truth lies somewhere between these two extreme interpretations; some short chains might originate from $^{288}$115, while the others are from $^{289}$115. For a particular decay chain, however, it is not possible to make a definite assignment.

Besides D3, also T4, D4, and B3 have a rather poor agreement in either interpretation. The $E_2$ of chain D4 also lies outside the typical window for $\alpha$ energies of $^{284}$113, and $E_1$ of B3 lies outside the typical window for $\alpha$ energies of $^{288}$115. The rather short correlation time of the observed fission event of chain D4 is also striking, as well as both decay times for B3. These chains might represent decay sequences stemming from isomeric states in the nuclei $^{288}$115 and/or $^{289}$115. As a side remark, the decay times for B3 actually seem to fit best with the half-lives of chains assigned to the 4$n$ evaporation channel $^{287}$115.

## 5. Cross section considerations

The hitherto presented scenarios can be propagated into cross sections for creation of various nuclear states. Table 6 provides measured cross sections for the two decay scenarios 1 and 2 shown in Fig. 2.

For 'scenario 1', where *all* short chains are associated with $^{289}$115, the numbers would be consistent with Fig. 4 of Ref. [12]. This implies rather high values for the 2$n$ channel, and a ratio of maximum production cross-sections $R_\sigma = \sigma(2n)/\sigma(3n) \approx 0.5$ (cf. Ref. [12] and Table 6). Such high relative or absolute yields of the production of the 2$n$ reaction channel $^{289}$115 are not necessarily consistent with expectations from nuclear reaction theory [48–50].

In 'scenario 2', the cross-section of the 2$n$ reaction channel $^{289}$115 amounts to $\approx$ 1 pb at low excitation energies $E^* \approx 34$ MeV. This corresponds to $\approx$10% of the maximum cross-section of the 3$n$-channel around $E^* = 37$ MeV and is in line with theoretical expectations.

## 6. Nuclear structure considerations

The proposed interpretations suggest the presence of more than one decay sequence in either $^{289}$115 or $^{288}$115, or both, where isomeric states give rise to different lifetimes and decay energies. Nuclear structure models support this suggested trend in the case of $^{289}$115, for which nuclear structure calculations are feasible. Fig. 3 provides proton single-particle energies predicted by macroscopic–microscopic model parameterisations [51–53] and a Skyrme energy density functional [54–56]. Independent of the model or the parameterisation, the nuclear shape is predicted to change from near-sphericity towards prolate deformation along the decay chain $^{289}115 \rightarrow {}^{285}113 \rightarrow {}^{281}$Rg. Most interestingly, however, all models suggest the same decay *pattern*, namely two independent $\alpha$-decay sequences: Exemplified in Fig. 3(b), once $^{289}$115 is created as final fusion-evaporation product, excited states will decay by electromagnetic radiation into *either* a high-$\Omega$ positive-parity state (here: [606]13/2) *or* a low-$\Omega$ negative-parity state (here: [541]1/2). The two families (high-$\Omega$ and low-$\Omega$) of Nilsson orbitals are likely to remain separate for the daughter $^{285}$113 and grand-daughter $^{281}$Rg, giving rise to two parallel $\alpha$-decay

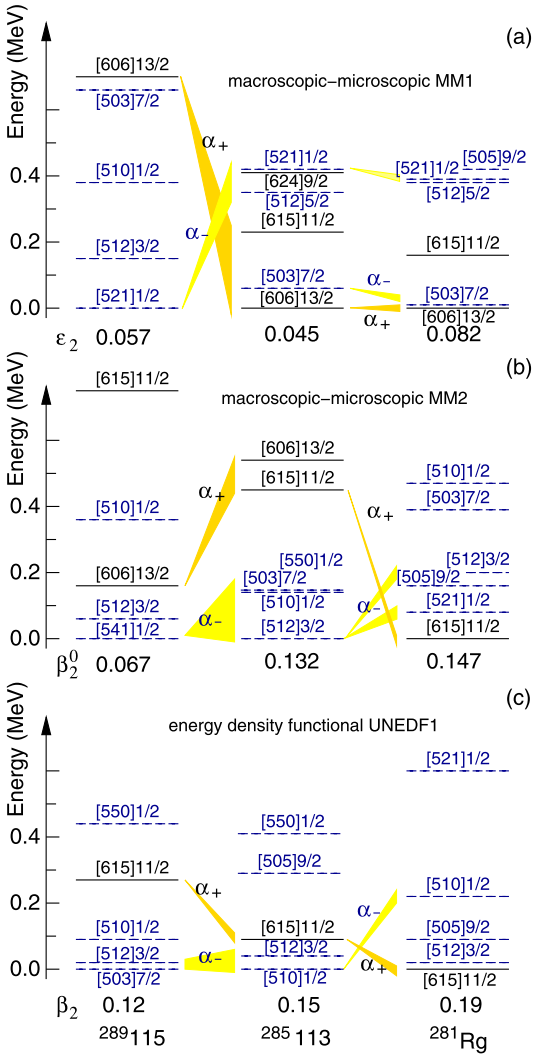


Fig. 3. (Colour online.) Nuclear structure predictions of low-lying states in $^{289}115$, $^{285}113$, and $^{281}$Rg. Panels (a) and (b) are based on two different macroscopic–microscopic approaches, MM1 [51,52] and MM2 [53]. Panel (c) originates from the self-consistent Skyrme energy density functional UNEDF1 [55,56]. The results from UNEDF1$^{\mathrm{SO}}$ are similar to MM2 [56]. Proton single-particle states are labelled with their asymptotic Nilsson quantum numbers $[Nn_z\Lambda]\Omega$. Full (black) lines represent positive-parity states, dashed (blue) lines negative-parity states. Selected $\alpha$-decay sequences among high-$\Omega$ positive-parity ($\alpha_+$) and low-$\Omega$ negative-parity ($\alpha_-$) states are indicated by shaded areas. $\epsilon_2$, $\beta_2^0$, $\beta_2$, respectively, denote predicted quadrupole deformations.

sequences. Detailed predictions are highly model dependent and it is currently not possible to say which predicted decay sequence can be associated with the observed ones, but the general trend with two different decay sequences in $^{289}115$ favours an interpretation which lies between scenario 1 and scenario 2, i.e. where some short chains are from $^{289}115$ and some from $^{288}115$, with D3 forming a separate $^{289}115$ sequence.

## 7. Summary

In summary, seven new recoil-$\alpha$–($\alpha$)-SF chains were observed following the fusion-evaporation reaction $^{48}$Ca + $^{243}$Am. An assessment of these seven decay chains together with seven previously published [8,12] chains suggests revisions to the initial assignments of short element 115 chains to the isotope $^{289}$115: Instead, it is likely that some of these chains start from the isotope $^{288}$115 and proceed through either SF or EC decay branches of $^{284}$113 and $^{280}$Rg. The remaining short chains can account for two separate decay sequences of the isotope $^{289}$115. Clearly, more high-quality spectroscopic data near the barrier of the $^{48}$Ca + $^{243}$Am reaction are needed to verify *any* proposed decay scenario of $^{288,289}$115.

## Acknowledgements

The authors would like to thank the ion-source and the accelerator staff at GSI. This work is supported by the European Community FP7 – Capacities ENSAR No. 262010, the Royal Physiographic Society in Lund, the Euroball Owners Committee, the Swedish Research Council, the German BMBF, the U.S. Department of Energy, Office of Science, under Award Numbers DOE-DE-NA0002574 (the Stewardship Science Academic Alliances program) and DE-SC0008511 (NUCLEI SciDAC-3 Collaboration), and the UK Science and Technology Facilities Council.

## Appendix A. Description of figure-of-merit (FoM)

A $\mathrm{FoM}_j^{(n)}$, defined for each correlation time $t_j^{(n)}$ in decay step $j = 1, 2, 3$ of the chain identified by the number $n$, is calculated as the value of a probability density function for a reference data set. The geometric mean of $\mathrm{FoM}_j^{(n)}$ over all available steps $j$ in chain $n$ defines the $\mathrm{FoM}_{geom}^{(n)}$ for that chain. The arithmetic mean of $\mathrm{FoM}_{geom}^{(n)}$ over all $N$ chains defines the FoM for the data set with respect to the interpretation under consideration.

The reference data set can be the same as the one to examine. In this case the task of the test is to provide a measure of the internal congruence of the data set; each chain is evaluated with respect to the averages from the entire data set. If the individual chains all deviate strongly from the average data, the FoM value will be low. If the chains are all too similar to their average behaviour, the FoM will be high. Such a test is similar to the one proposed by Schmidt [39]. Note, however, that a low $\sigma_\theta$ corresponds to a large FoM and vice versa.

The reference data can also be an external set of chains. In this case the test gives an indication of how well the different data sets overlap. If the chains that are tested have either much longer or much shorter half-lives compared to the reference, the FoM will be low.

The probability density function for a selected reference data set is constructed from $N$ reference chains. Presumably, these reference chains originate from an exponential distribution characterised by an average lifetime $\tau$. This $\tau$ is not known precisely, but has an uncertainty. The probability density function used when evaluating the FoM should take this uncertainty into account, which leads to a smearing. To do this, we did not use the error bars associated with values of $\tau$, but instead the underlying likelihood functions. Examples of likelihood functions, as given by Eq. (16) in [37] but normalised such that they also serve as probability density functions, are shown in Fig. 4. The smeared probability density function is constructed as follows.

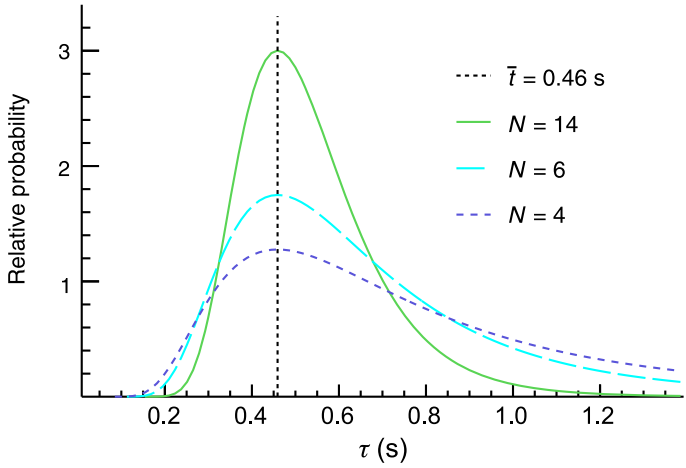


Fig. 4. (Colour online.) Likelihood functions for $\tau$ if different number of decay chains $N$ are measured to have an average lifetime $\bar{t} = \bar{t}_1 = 0.459$ s. The (green) solid line corresponds to the $\tau$ likelihood function for decay step $j = 1$ in the data set of fourteen short chains. The functions are normalised such that the integral on the interval [0,inf] is one.

1. For each step $j$, the average experimental lifetime $\bar{t}_j$ is calculated, and the number of available lifetimes $N_j$ is noted.
2. For each step $j$, the likelihood function for the true lifetime $\tau_j$, given by $N_j$ and $\bar{t}_j$, is determined.
3. For each step $j$, a $\tau_j$ is selected with a probability governed by the likelihood function for $\tau_j$, and then a set of $N_j$ lifetimes are generated from the exponential distribution defined by this $\tau_j$. This procedure is repeated until a smooth histogram emerges.

The corresponding analytic expression for the smeared probability density function for step $j$, using a reference data set with $N_j$ data points and average lifetime $\bar{t}_j$ in step $j$,

$$f(t) = t(N_j - 1)\frac{(N_j\bar{t}_j)^{N_j-1}}{(N_j\bar{t}_j + t)^{N_j}} \text{ (plotted in Fig. 5)}, \tag{A.1}$$

is obtained by weighting an exponential distribution $g(t) = \frac{t}{\tau}e^{-\frac{t}{\tau}}$ with the normalised likelihood function for $\tau$

$$h(\tau) = \frac{N^{N-1}}{(N-2)!}\frac{\bar{t}^{N-1}}{\tau^N}e^{-\frac{N\bar{t}}{\tau}} \text{ (plotted in Fig. 4)}. \tag{A.2}$$

The histogram emerging from the step-wise Monte Carlo procedure as well as the analytic expression $f(t)$, for the first step of the fourteen short chains, are shown in Fig. 5. For comparison, also $g(t)$ and $f(t)$ based on references consisting of $N = 4, 6$ chains are shown. The $\text{FoM}_j^n$ in chain $n$ is defined as $f(t_j^{(n)})$ (with the parameters $\bar{t}_j$ and $N_j$ from the reference data set) for the measured lifetime $t_j^{(n)}$.

To decide whether a FoM indicates congruence or not, it is compared to the distribution of FoM values that result when the same method is applied to a very large number of sets of chains generated by a Monte Carlo method to mimic the basic properties of the set of fourteen short chains. One method would be to generate sets of fourteen random numbers from exponential

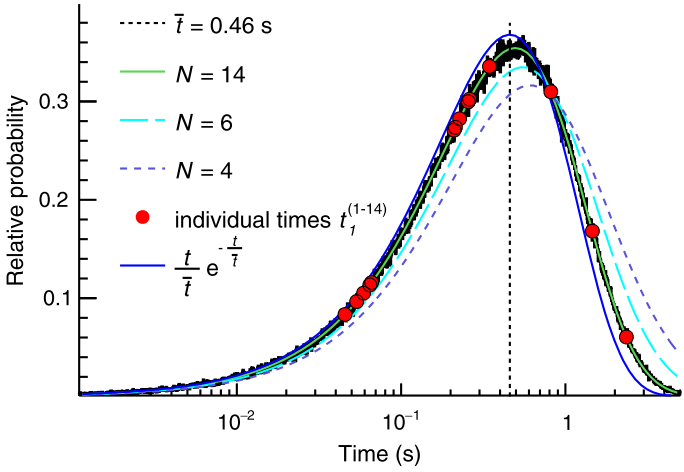


Fig. 5. (Colour online.) Relative probability for times $t$ that originate from an exponential distribution with a decay constant that is estimated from a low-statistics measurement (black). The number of data points used for determination of the likelihood function of the decay constant $\tau$ is $N = N_1 = 14$ and the corresponding average lifetime is $\bar{t} = \bar{t}_1 = 0.459$ s. The histogram is based on $10^5$ simulated sets of chains. The analytic expression (Eq. (A.1)) for the corresponding probability density function (solid line, light green) is also shown. For reference, the probability density function for times from an exponential decay with a known decay constant is shown (solid line, dark blue). Probability density functions for cases where the lifetime was determined from $N = 6$ and $N = 4$ data points are also shown. The fourteen markers (circular, red) indicate the individual fourteen lifetimes $t_1^{(1-14)}$ in decay step $j = 1$ of the fourteen short chains and their corresponding $\text{FoM}_1^{(1-14)}$.

distributions $g(t)$ characterised by the values $\bar{t}_j$. However, it was decided to take into account the uncertainty in $\bar{t}_j$ also when generating sets of chains. The chains were generated in the following way:

1. For the first decay step, a random $\tau_1$ was picked according to the $\tau$ likelihood function $h(\tau)$ (see Fig. 4). Fourteen random lifetimes from the exponential distribution $g(t)$ defined by this $\tau_1$ were generated.
2. For the second decay step, a random $\tau_2$ was picked according to the $\tau$ likelihood function $h(\tau)$. Fourteen random lifetimes from the exponential distribution $g(t)$ defined by this $\tau_2$ were generated.
3. For the third decay step, a random $\tau_3$ was picked according to the $\tau$ likelihood function $h(\tau)$. Ten random lifetimes from the exponential distribution $g(t)$ defined by this $\tau_3$ were generated.
4. The generated lifetimes were collected in fourteen chains – ten with three lifetimes, and four with two lifetimes.

In this way, $10^5$ sets of chains were created. The FoM for the generated sets of chains were evaluated in the same way as the experimental data. Fig. 6 shows the FoM distribution for these simulated chains, and the corresponding upper and lower 90% confidence limits. Also the $\text{FoM}_{geom}$ distribution for a single chain is shown with the corresponding lower 90% limit. This is done for two different cases – for recoil-$\alpha$-SF and recoil-$\alpha$–$\alpha$-SF chains. The confidence limits for all relevant cases were calculated in this way.

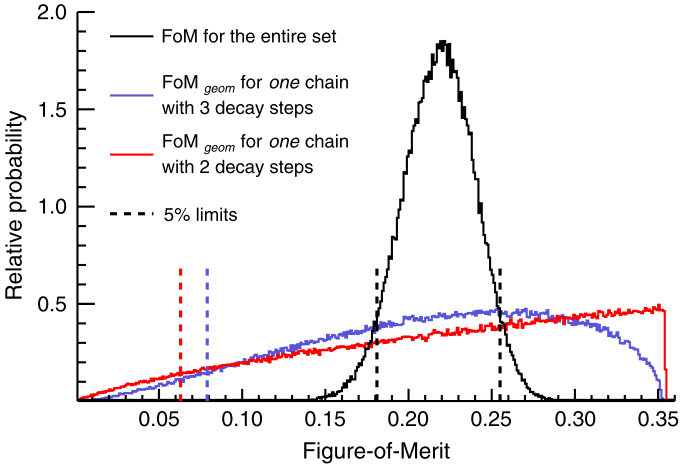


Fig. 6. (Colour online.) Relative probability of FoM values: FoM for an entire data set of fourteen chains with similar characteristics as the experimental fourteen short chains (black), $\mathrm{FoM}_{geom}$ for *one* of the recoil-$\alpha$–$\alpha$-SF chains (blue), and $\mathrm{FoM}_{geom}$ for *one* of the recoil-$\alpha$-SF chains (red). A selection of the respective 5% limits (dashed lines) are also shown. The histograms are based on $10^5$ simulated sets of chains.

## References


[1] R.C. Barber, P.J. Karol, H. Nakahara, E. Vardaci, E. Vogt, Pure Appl. Chem. 83 (7) (2011) 1485.
[2] P.J. Karol, R.C. Barber, B.M. Sherrill, E. Vardaci, T. Yamazaki, Pure Appl. Chem. (January 2016), http://dx.doi.org/10.1515/pac-2015-0502, ISSN (Online) 1365-3075, ISSN (Print) 0033-4545.
[3] P.J. Karol, R.C. Barber, B.M. Sherrill, E. Vardaci, T. Yamazaki, Pure Appl. Chem. (January 2016), http://dx.doi.org/10.1515/pac-2015-0501, ISSN (Online) 1365-3075, ISSN (Print) 0033-4545.
[4] A. Bohr, B.R. Mottelson, Nuclear Structure, Volume II, W.A. Benjamin, Inc., Massachusetts, 1975.
[5] G.T. Seaborg, W.D. Loveland, The Elements Beyond Uranium, Wiley-Interscience, New York, 1990.
[6] R.-D. Herzberg, P.T. Greenlees, Prog. Part. Nucl. Phys. 61 (2008) 674.
[7] D. Rudolph, et al., Phys. Rev. Lett. 111 (2013) 112502.
[8] J.M. Gates, et al., Phys. Rev. C 92 (2015) 021301(R).
[9] Yu.Ts. Oganessian, et al., Phys. Rev. Lett. 104 (2010) 142502.
[10] Yu.Ts. Oganessian, Radiochim. Acta 99 (2011) 429.
[11] Yu.Ts. Oganessian, et al., Phys. Rev. Lett. 108 (2012) 022502.
[12] Yu.Ts. Oganessian, et al., Phys. Rev. C 87 (2013) 014302.
[13] Yu.Ts. Oganessian, et al., Phys. Rev. C 87 (2013) 054621.
[14] J. Khuyagbaatar, et al., Phys. Rev. Lett. 112 (2014) 172501.
[15] K. Morita, et al., J. Phys. Soc. Jpn. 81 (2012) 103201.
[16] Yu.Ts. Oganessian, et al., Phys. Rev. C 69 (2004) 021601(R).
[17] M. Schädel, Eur. Phys. J. D 45 (2007) 67.
[18] A. Semchenkov, et al., Nucl. Instrum. Methods B 266 (2008) 4153.
[19] J.M. Gates, et al., Phys. Rev. C 83 (2011) 054618.
[20] E. Jäger, Ch.E. Düllmann, J. Khuyagbaatar, J. Krier, M. Schädel, T. Torres, A. Yakushev, J. Radioanal. Nucl. Chem. 299 (2014) 1073.
[21] J. Runke, et al., J. Radioanal. Nucl. Chem. 299 (2014) 1081.
[22] J.F. Ziegler, Nucl. Instrum. Methods A 219 (2004) 1024.
[23] W.D. Myers, W.J. Swiatecki, Nucl. Phys. A 601 (1996) 141.
[24] J. Khuyagbaatar, et al., Nucl. Instrum. Methods A 689 (2012) 40.
[25] U. Forsberg, et al., Acta Phys. Pol. 43 (2012) 305.
[26] L.-L. Andersson, et al., Nucl. Instrum. Methods A 622 (2010) 164.
[27] K.E. Gregorich, Nucl. Instrum. Methods A 711 (2013) 47.

[28] P. Golubev, et al., Nucl. Instrum. Methods A 723 (2013) 55.
[29] J. Hoffmann, et al., GSI scientific report 2011, GSI report 2012-1, 2012.
[30] U. Forsberg, et al., EPJ Web Conf. 66 (2014) 02036.
[31] D. Rudolph, et al., Acta Phys. Pol. B 45 (2014) 263.
[32] D. Rudolph, et al., J. Radioanal. Nucl. Chem. 303 (2015) 1185.
[33] U. Forsberg, et al., to be published.
[34] L.G. Sarmiento, L.-L. Andersson, D. Rudolph, Nucl. Instrum. Methods A 667 (2012) 26.
[35] L.G. Sarmiento, et al., in: Proc. 10th Latin American Symposium on Nuclear Physics and Applications, X LASNPA, PoS (2014) 057.
[36] D. Rudolph, L.G. Sarmiento, U. Forsberg, AIP Conf. Proc. 1681 (2015) 030015.
[37] K.-H. Schmidt, C.-C. Sahm, K. Pielenz, H.-G. Clerc, Z. Phys. A 316 (1984) 19.
[38] Yu.Ts. Oganessian, et al., Phys. Rev. C 83 (2011) 054315.
[39] K.-H. Schmidt, Eur. Phys. J. A 8 (2000) 141.
[40] Ch.E. Düllmann, et al., Phys. Rev. Lett. 104 (2010) 252701.
[41] R. Smolańczuk, J. Skalski, A. Sobiczewski, Phys. Rev. C 52 (1995) 1871.
[42] M. Warda, J.L. Egido, Phys. Rev. C 86 (2012) 014322.
[43] A. Staszczak, A. Baran, W. Nazarewicz, Phys. Rev. C 87 (2013) 024320.
[44] D.C. Hoffman, M.R. Lane, Radiochim. Acta 70/71 (1995) 135.
[45] F.P. Heßberger, EPJ Web Conf. 66 (2014) 02048.
[46] A.V. Karpov, V.I. Zagrebaev, Y. Martinez Palenzuela, L. Felipe Ruiz, W. Greiner, Int. J. Mod. Phys. E 21 (2012) 1250013.
[47] V. Zagrebaev, A. Karpov, W. Greiner, J. Phys. Conf. Ser. 420 (2013) 012001, Acta Phys. Pol. 45 (2014) 291.
[48] V.I. Zagrebaev, Nucl. Phys. A 734 (2004) 164.
[49] K. Siwek-Wilczyńska, T. Cap, M. Kowal, A. Sobiczewski, J. Wilczyński, Phys. Rev. C 86 (2012) 014611.
[50] W. Reisdorf, M. Schädel, Z. Phys. A 343 (1992) 47.
[51] B.G. Carlsson, I. Ragnarsson, Phys. Rev. C 74 (2006) 011302.
[52] S.G. Nilsson, C.F. Tsang, A. Sobiczewski, Z. Szymański, S. Wycech, C. Gustafson, I.-L. Lamm, P. Möller, B. Nilsson, Nucl. Phys. A 131 (1969) 1.
[53] A. Parkhomenko, A. Sobiczewski, Acta Phys. Pol. B 35 (2004) 2447.
[54] S. Ćwiok, W. Nazarewicz, P.H. Heenen, Phys. Rev. Lett. 83 (1999) 1108.
[55] M. Kortelainen, J. McDonnell, W. Nazarewicz, P.-G. Reinhard, J. Sarich, N. Schunck, M.V. Stoitsov, S.M. Wild, Phys. Rev. C 85 (2012) 024304.
[56] Yue Shi, D.E. Ward, B.G. Carlsson, J. Dobaczewski, W. Nazarewicz, I. Ragnarsson, D. Rudolph, Phys. Rev. C 90 (2014) 014308.